Supplementary information to accompany

Tetraoxolene-bridged rare-earth complexes: a radical-bridged dinuclear Dy single-molecule magnet†

William R. Reed,[a] Maja A. Dunstan,[a] Robert W. Gable,[a] Wasinee Phonsri,[b] Keith S. Murray,[b] Richard A. Mole[c] and Colette Boskovic*[a]

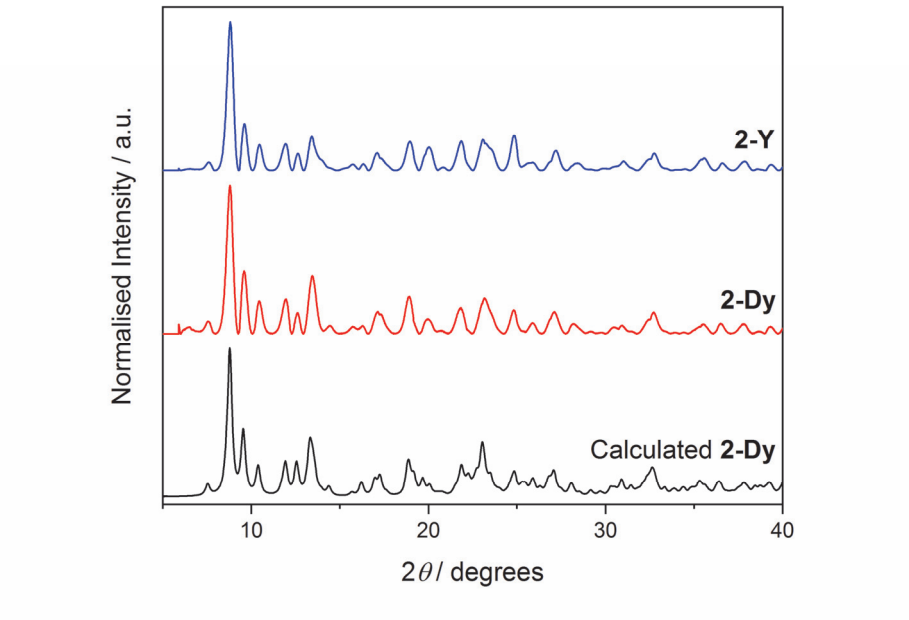

Fig. S1 Powder X-ray diffraction data for **2-RE** (RE = Y, Dy) with the powder pattern calculated from the single crystal diffraction data.

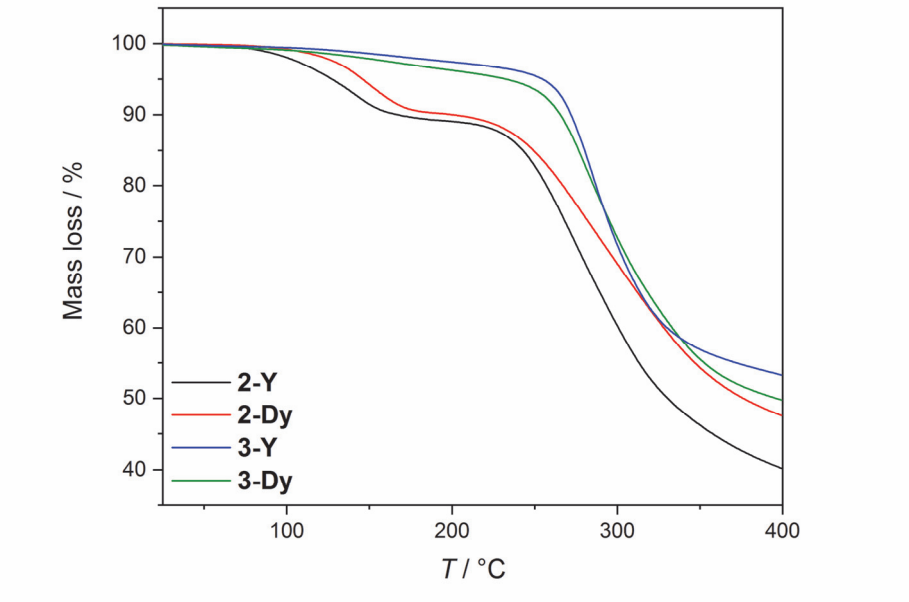

Fig. S2 Thermogravimetric analysis data for **2-RE** and **3-RE** (RE = Y, Dy)

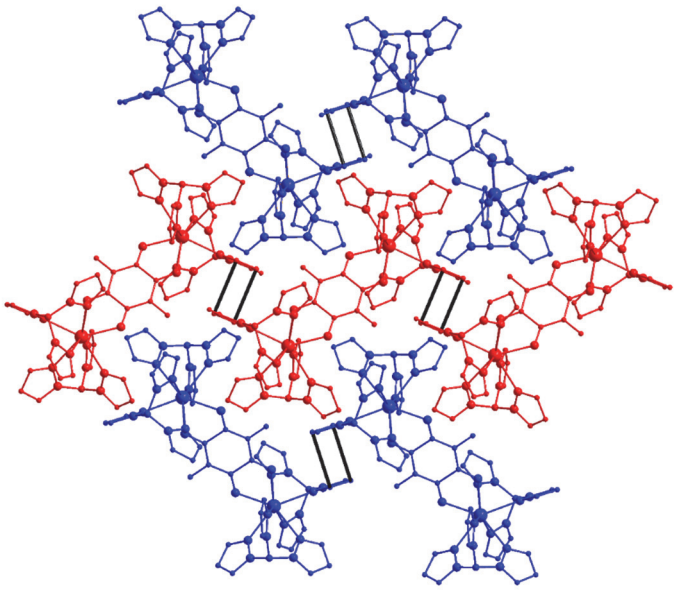

Fig. S3 Crystal packing diagram along the *a* axis for **1-RE** with intermolecular interactions in black.

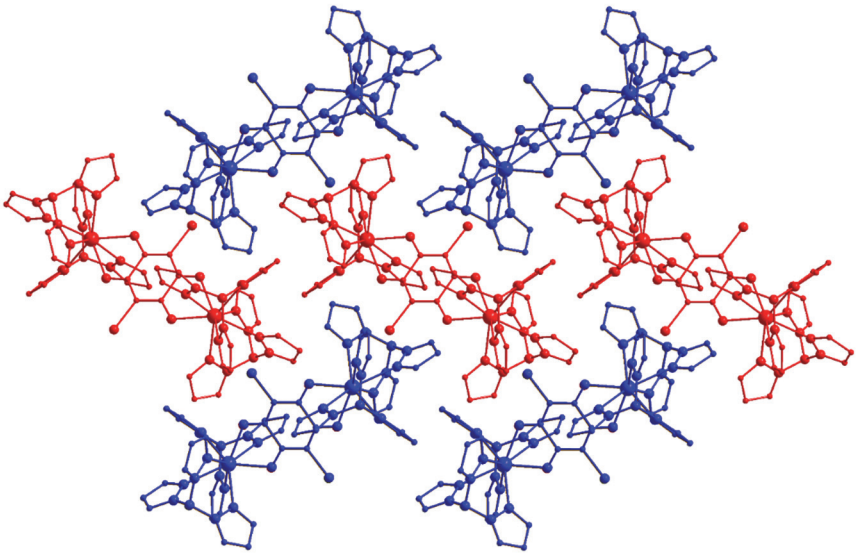

Fig. S4 Crystal packing diagram along the *a* axis for **2-RE.**

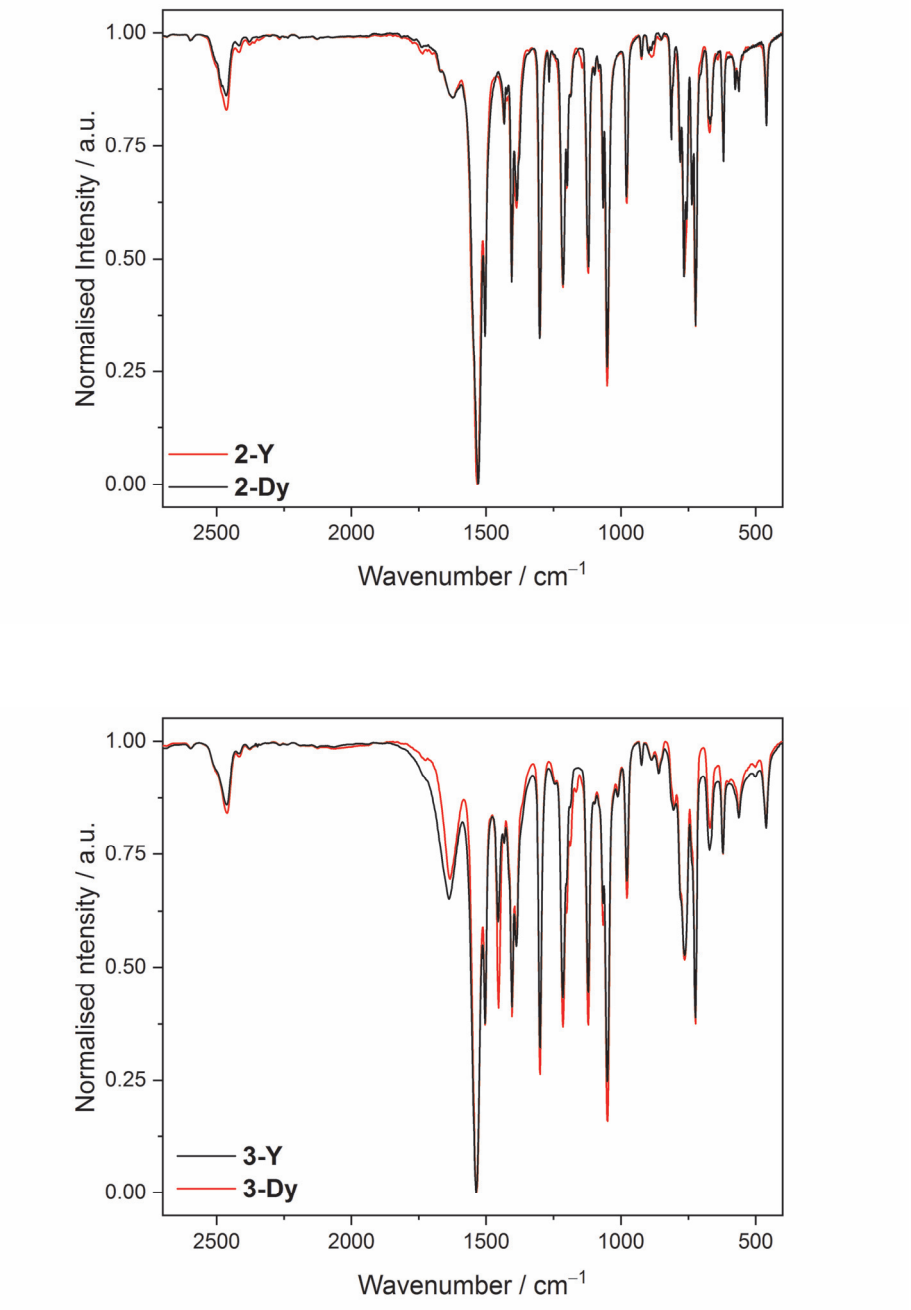

Fig. S5 IR spectra of **2-Y**, **2-Dy** (above), **3-Y** and **3-Dy** (below) as pressed KBr disks.

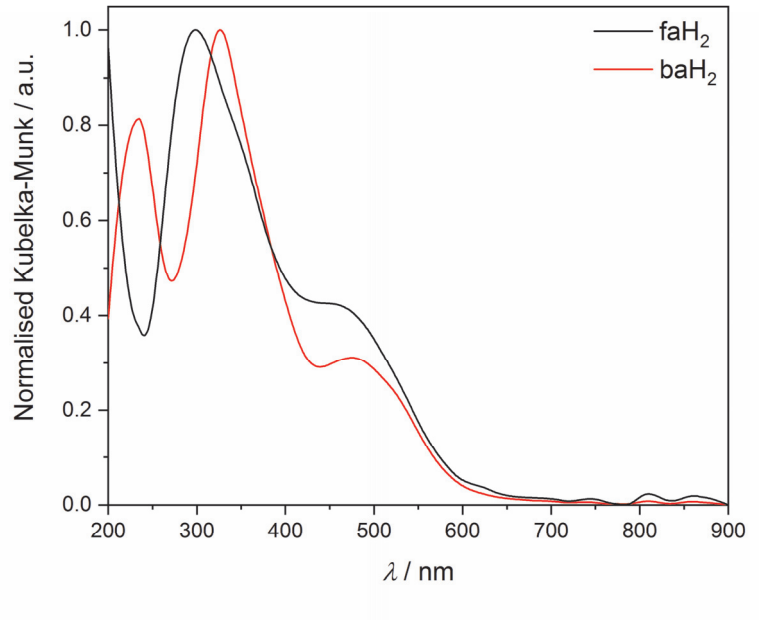

Fig. S6 Solid state diffuse reflectance UV-visible spectra measured for samples of fluoranilic and bromanilic acid dispersed in KBr.

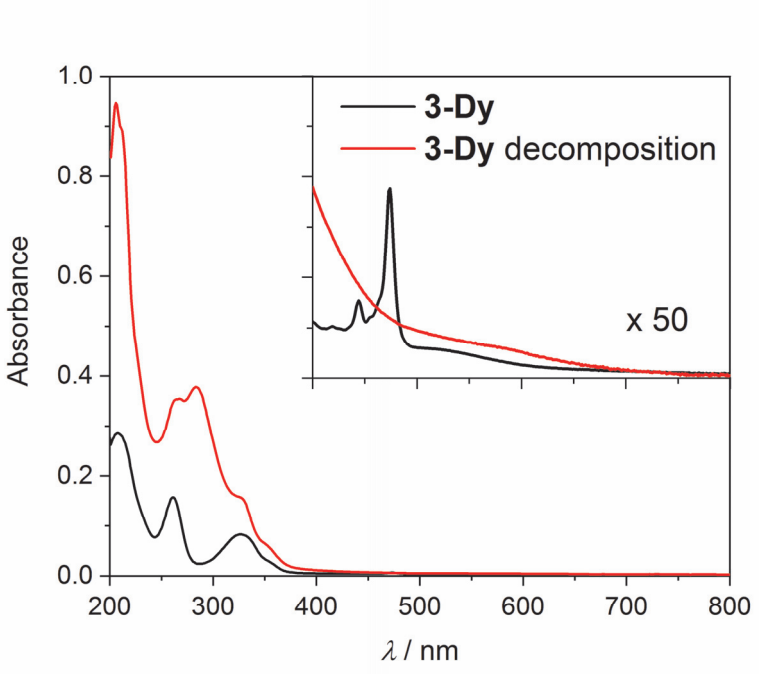

Fig. S7 UV-visible spectra measured for a solution of **3-Dy** in MeCN before (black) and after (red) exposure to atmosphere.

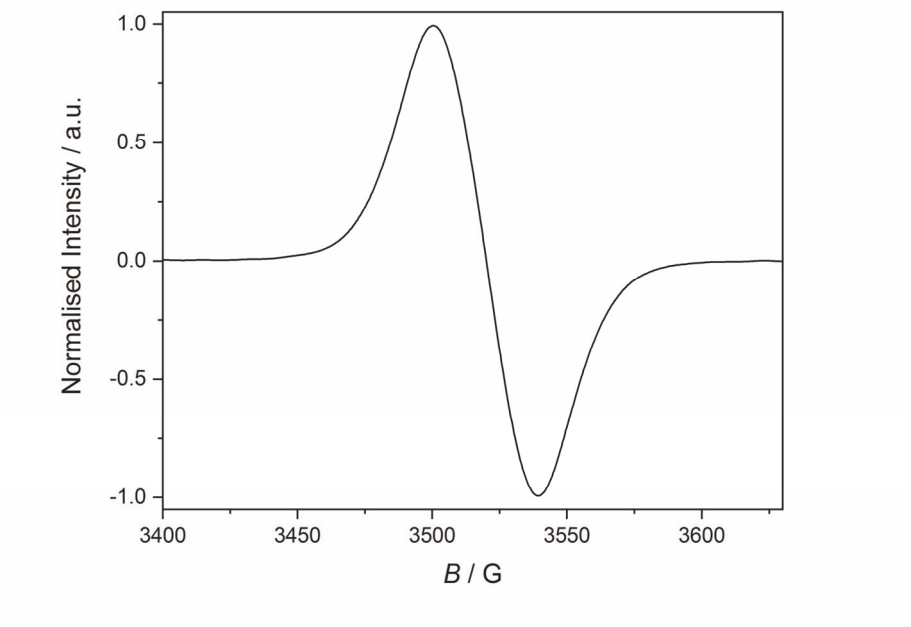

Fig. S8 Room temperature X-band EPR spectrum of a powder sample of **3-Y**.

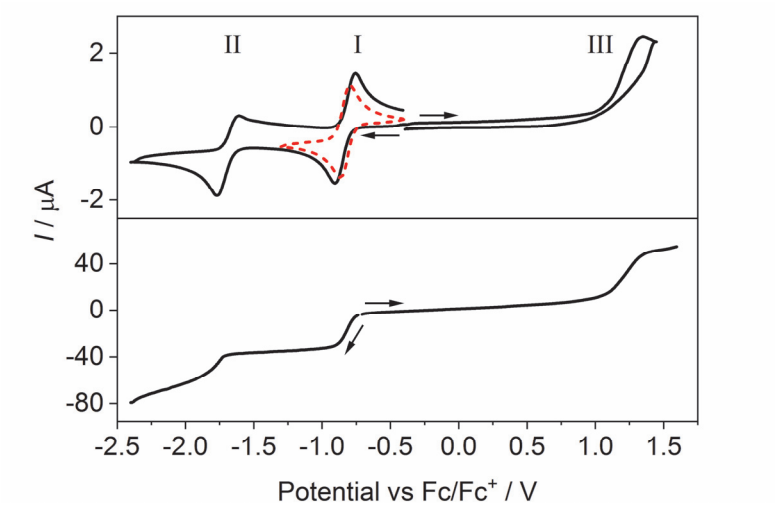

Fig. S9 Cyclic and RDE voltammograms of **2-Y** (0.5 mM in MeCN with 0.25 M Bu_4NPF_6) obtained with a 3 mm diameter glassy carbon working electrode at a scan rate of 100 or 20 mVs^{-1}, for CV and RDE, respectively. The dashed red lines plot the voltammograms measured with a switching potential immediately past the first reduction to probe reversibility. The anodic and cathodic regions were scanned separately as indicated by the arrows.

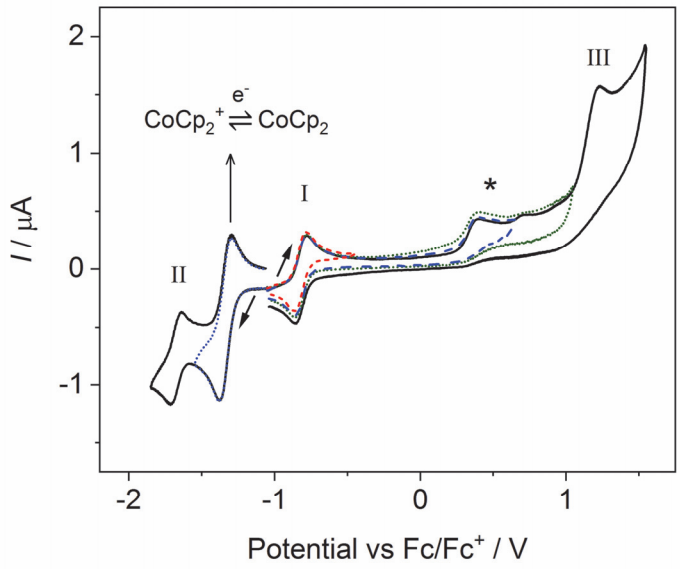

Fig. S10 Cyclic voltammogram of **3-Dy** (approximately 0.5 mM in MeCN with 0.1 M Bu_4NPF_6) obtained with a 1 mm diameter glassy carbon working electrode at a scan rate of 100 mVs^{-1}. The dashed coloured lines plot the voltammograms measured with a switching potential immediately past each consecutive process to probe reversibility. The anodic and cathodic regions were scanned separately as indicated by the arrows. The processes marked with an asterisk are associated with decomposition products.

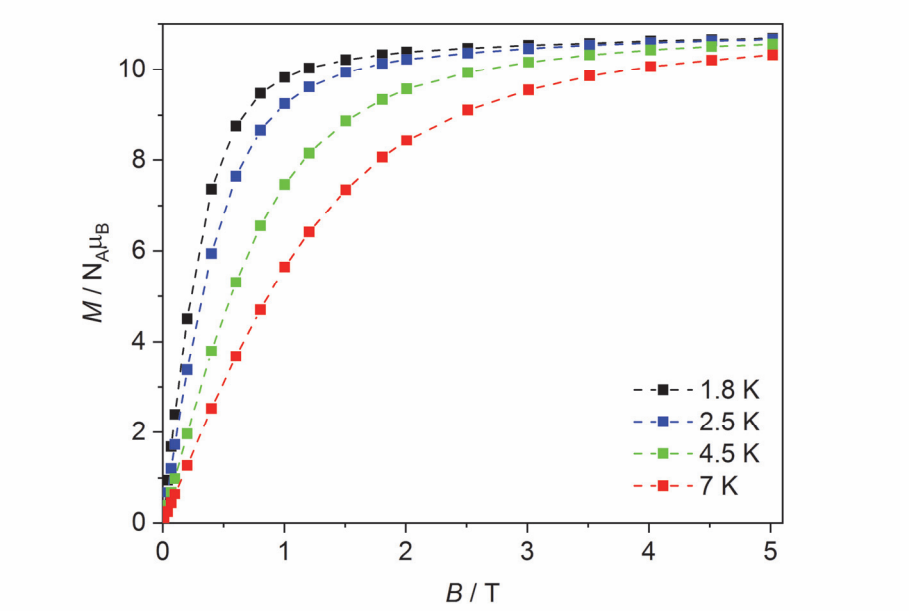

Fig. S11 Plots of magnetisation versus field for **2-Dy**. The lines are a guide for the eye.

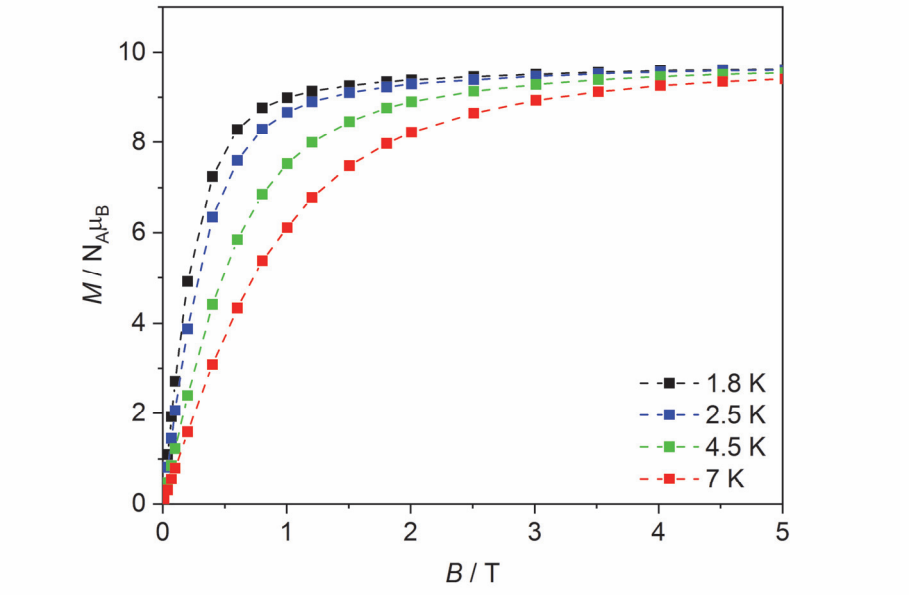

Fig. S12 Plots of magnetisation versus field for **3-Dy**. The lines are a guide for the eye.

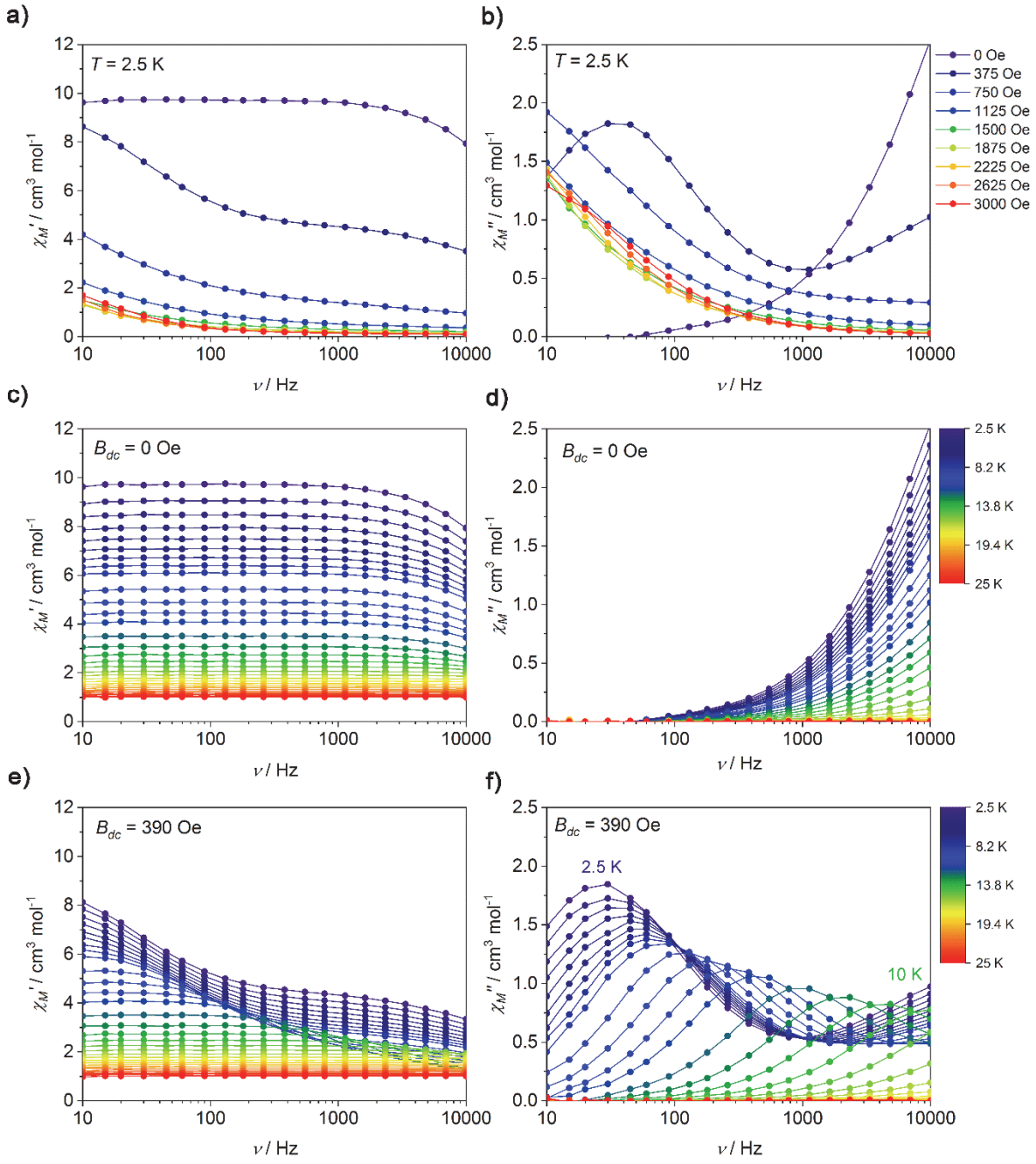

Fig. S13 In-phase χ_M' (left) and out-of-phase χ_M'' (right) ac susceptibility data for **2-Dy**; field scans at 2.5 K (top); temperature scans with $B_{dc} = 0$ (middle); temperature scans with $B_{dc} = 390$ Oe (bottom, maxima in χ_M'' evident within the frequency range for the temperature range 2.5–10 K). Lines are a guide for the eye.

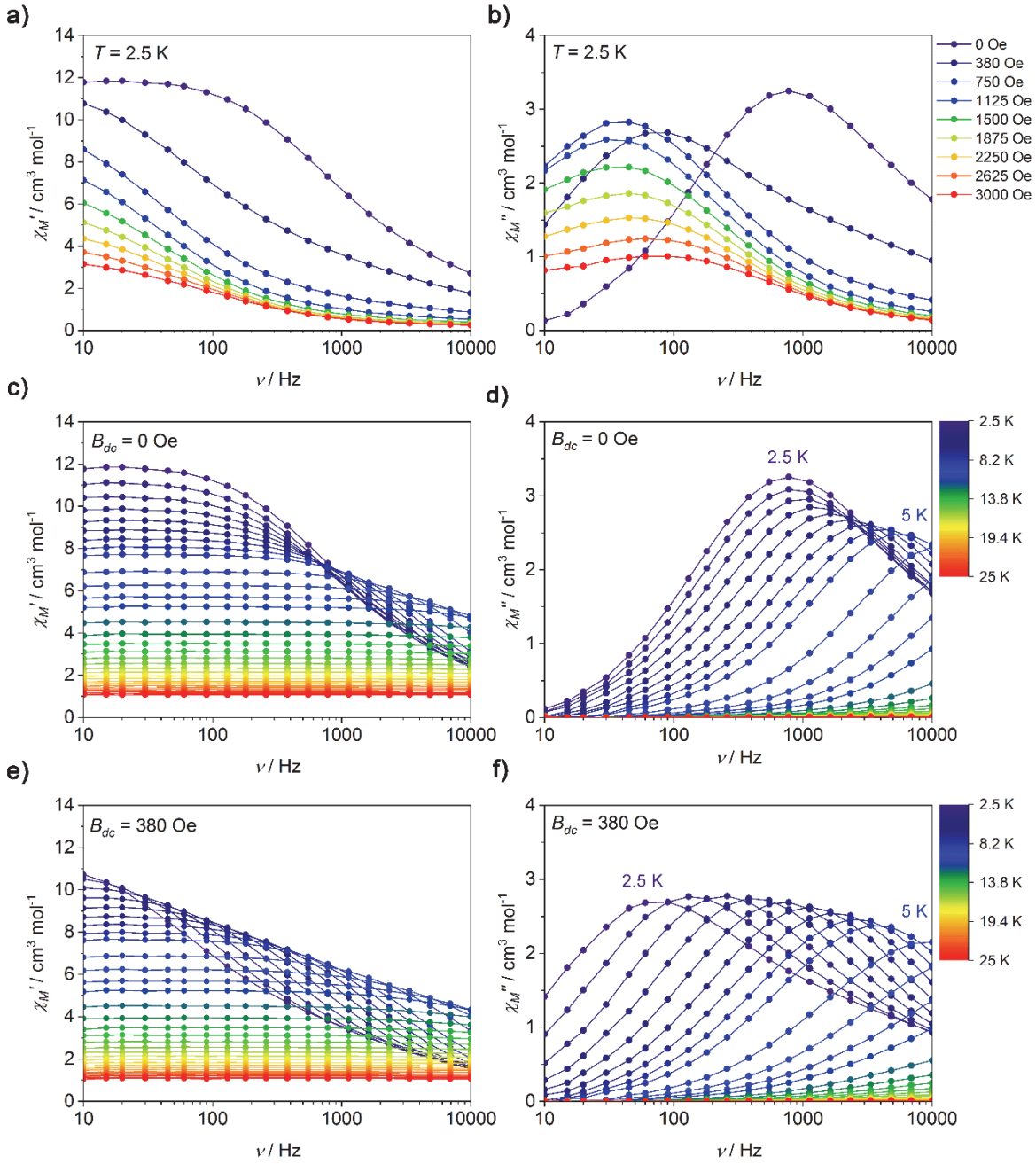

Fig. S14 In-phase χ_M' (left) and out-of-phase χ_M'' (right) ac susceptibility data for **3-Dy**; field scans at 2.5 K (top); temperature scans with $B_{dc} = 0$ (middle, maxima in χ_M'' evident within the frequency range for the temperature range 2.5–5 K); temperature scans with B_{dc} = 380 Oe (bottom, maxima in χ_M'' evident within the frequency range for the temperature range 2.5–5 K). Lines are a guide for the eye.

Table S1 The relaxation time τ and α-values obtained from fitting the isotherms in the out-of-phase magnetic susceptibility[a] to the Debye equation for **2-Dy** and **3-Dy.**

	2-Dy, B_{dc} = 390 Oe		**3-Dy**, B_{dc} = 0 Oe		**3-Dy**, B_{dc} = 380 Oe	
T / K	τ / s	α	τ / s	α	τ / s	α
2.50	$(5.89 \pm 0.11) \times 10^{-3}$	0.249 ± 0.008	$(1.85 \pm 0.05) \times 10^{-4}$	0.290 ± 0.013	$(2.02 \pm 0.04) \times 10^{-3}$	0.332 ± 0.017
2.69	$(5.07 \pm 0.06) \times 10^{-3}$	0.256 ± 0.006	$(1.64 \pm 0.05) \times 10^{-4}$	0.281 ± 0.014	$(1.09 \pm 0.18) \times 10^{-4}$	0.343 ± 0.012
2.88	$(4.32 \pm 0.05) \times 10^{-3}$	0.247 ± 0.006	$(1.40 \pm 0.03) \times 10^{-4}$	0.300 ± 0.013	$(5.86 \pm 0.13) \times 10^{-4}$	0.325 ± 0.012
3.07	$(3.76 \pm 0.04) \times 10^{-3}$	0.243 ± 0.005	$(1.12 \pm 0.03) \times 10^{-4}$	0.285 ± 0.012	$(3.42 \pm 0.08) \times 10^{-4}$	0.306 ± 0.011
3.25	$(3.22 \pm 0.05) \times 10^{-3}$	0.225 ± 0.009	$(8.78 \pm 0.19) \times 10^{-5}$	0.268 ± 0.010	$(2.14 \pm 0.03) \times 10^{-4}$	0.304 ± 0.007
3.44	$(2.78 \pm 0.05) \times 10^{-3}$	0.205 ± 0.011	$(6.76 \pm 0.22) \times 10^{-5}$	0.234 ± 0.013	$(1.36 \pm 0.02) \times 10^{-4}$	0.293 ± 0.006
3.63	$(2.43 \pm 0.05) \times 10^{-3}$	0.186 ± 0.013	$(5.13 \pm 0.15) \times 10^{-5}$	0.225 ± 0.012	$(9.05 \pm 0.30) \times 10^{-5}$	0.256 ± 0.013
3.82	$(2.14 \pm 0.05) \times 10^{-3}$	0.165 ± 0.016	$(3.90 \pm 0.13) \times 10^{-5}$	0.212 ± 0.013	$(6.27 \pm 0.21) \times 10^{-5}$	0.253 ± 0.013
4.01	$(1.82 \pm 0.05) \times 10^{-3}$	0.159 ± 0.017	$(2.99 \pm 0.11) \times 10^{-5}$	0.200 ± 0.014	$(4.46 \pm 0.16) \times 10^{-5}$	0.252 ± 0.013
4.51	$(1.41 \pm 0.05) \times 10^{-3}$	0.0373 ± 0.0187	$(1.60 \pm 0.05) \times 10^{-5}$	0.171 ± 0.007	$(2.08 \pm 0.15) \times 10^{-5}$	0.248 ± 0.018
5.01	$(8.71 \pm 0.28) \times 10^{-4}$	0.0465 ± 0.0191	$(1.04 \pm 0.09) \times 10^{-5}$	0.135 ± 0.017	$(1.20 \pm 0.17) \times 10^{-5}$	0.249 ± 0.024
5.51	$(5.70 \pm 0.21) \times 10^{-4}$	0.0284 ± 0.0222	-	-	-	-
6.01	$(3.58 \pm 0.10) \times 10^{-4}$	0.0470 ± 0.0170	-	-	-	-
7.01	$(1.70 \pm 0.06) \times 10^{-4}$	0.0331 ± 0.0177	-	-	-	-
8.01	$(8.07 \pm 0.02) \times 10^{-4}$	0.0495 ± 0.0135	-	-	-	-
9.01	$(3.80 \pm 0.01) \times 10^{-4}$	0.0686 ± 0.0980	-	-	-	-
10.01	$(1.79 \pm 0.01) \times 10^{-4}$	0.0736 ± 0.0109	-	-	-	-

[a] magnetic data from Fig. S14f, Fig. S15d and f.

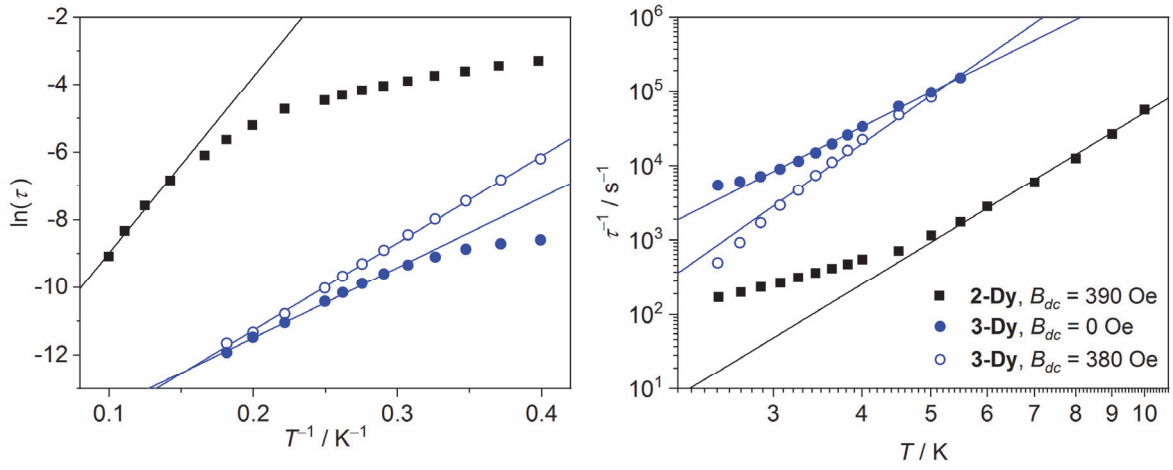

Fig. S15 Relaxation time plots for **2-Dy** (B_{dc} = 390 Oe, black) and **3-Dy** (B_{dc} = 0 Oe, blue closed circles; B_{dc} = 380 Oe, blue open circles): Arrhenius plot with fits for a purely Orbach process (left) and log-log plots with fits for a purely Raman process (right). Data obtained in the temperature ranges 2.5–10 K (**2-Dy**) and 2.5–5.0 K (**3-Dy**).

Table S2 Parameters of best fit obtained from fitting the ac relaxation data for **2-Dy** and **3-Dy** considering only an Orbach or Raman relaxation process.

	Orbach		**Raman**	
	τ_0 / s	U_{eff} / K	C /s K^{-n}	n
2-Dy, B_{dc} = 390 Oe	(6.76 ± 3.27) × 10^{-7}	52.2 ± 4.0	0.0836 ± 0.0443	5.79 ± 0.23
3-Dy, B_{dc} = 0 Oe	(1.60 ± 0.14) × 10^{-7}	20.8 ± 0.4	42.3 ± 7.7	4.81 ± 0.11
3-Dy, B_{dc} = 380 Oe	(7.40 ± 0.54) × 10^{-8}	25.8 ± 0.3	1.83 ± 0.57	6.70 ± 0.20

Table S3 The relaxation time τ and α-values obtained from fitting the isofield lines in the out-of-phase magnetic susceptibility at 2.5 K[a] to the Debye equation for **3-Dy.**

B_{dc} / T	τ / s	α
0.085	$(1.85 \pm 0.05) \times 10^{-4}$	0.290 ± 0.013
380	$(2.02 \pm 0.04) \times 10^{-3}$	0.332 ± 0.017
750	$(4.16 \pm 0.17) \times 10^{-3}$	0.392 ± 0.010
1125	$(4.71 \pm 0.08) \times 10^{-3}$	0.359 ± 0.005
1500	$(4.65 \pm 0.09) \times 10^{-3}$	0.357 ± 0.006
1875	$(4.23 \pm 0.12) \times 10^{-3}$	0.363 ± 0.008
2250	$(3.73 \pm 0.11) \times 10^{-3}$	0.374 ± 0.008
2625	$(3.06 \pm 0.11) \times 10^{-3}$	0.384 ± 0.010
3000	$(2.62 \pm 0.12) \times 10^{-3}$	0.407 ± 0.012

[a] magnetic data from Fig. S15b.

Discussion S1

The complete set of $\tau(T,H)$ data for **3-Dy** (Table S1, Table S3) were fit simultaneously to give relaxation parameters using the modification of Eq. 1 that incorporates the field-dependence:

$$\tau^{-1} = \tau_0^{-1} \exp\left(-U_{eff}/k_B T\right) + C' \frac{1+B_1 B^2}{1+B_2 B^2} T^n + A' B^4 T + \frac{1+D_1}{1+D_2 B^2} \quad \textbf{(S1)}$$

using the relationships $C = C' \frac{1+B_1 B^2}{1+B_2 B^2}$,[1] $A = A' B^4$,[2] and $\tau_{QTM}^{-1} = \frac{1+D_1}{1+D_2 B^2}$.[3]

A sensible fit of both the temperature- and field-dependence could only be obtained by considering all four relaxation pathways, with n fixed to 7 as values close to 7 gave the best fits (Fig. S15, Table S4). The field-dependent relaxation parameters in Eq. S1 (C, A and τ_{QTM}) were then calculated for the two fields (Table S4) and the resulting values used as initial parameters for fitting the individual $\tau(T)$ data sets at each field to Eq. 1, as discussed in the main text, to give the values presented in Table 3. This approach was employed due to the large number of parameters and the inability to get a fully satisfactory fit of the combined $\tau(T,H)$ data.

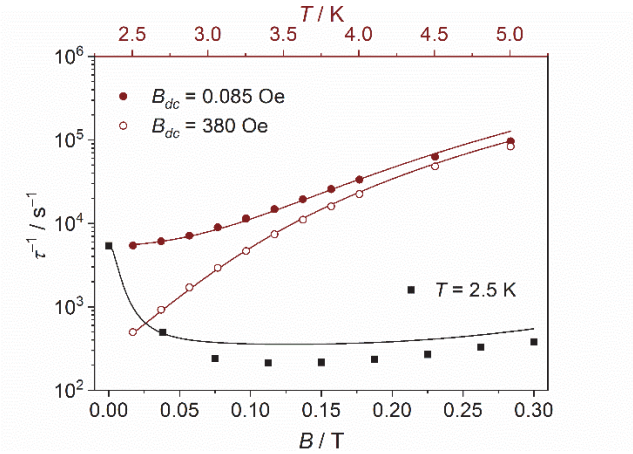

Fig. S16 Relaxation time plots for **3-Dy** showing the result (lines) of simultaneous fits of $\tau(T)$ data with B_{dc} = 0 (0.085) Oe (red filled circles) and 380 Oe (red empty circles) and $\tau(B)$ at 2.5 K (black squares).

Table S4 Relaxation parameters obtained from the simultaneous fit of all $\tau(T,B)$ data for **3-Dy** fitting to eq. S1 and the corresponding calculated values used as initial parameters for fitting $\tau(T)$ at both fields to eq. 1.

	Fit to all data	**B_{dc} = 0.085 Oe**	**B_{dc} = 380 Oe**
A' / s^{-1} T^{-4} K^{-1}	(1.03 ± 0.90) × 10^4	-	-
A / s^{-1} K^{-1}	-	5.37 × 10^{-17}	0.0215
τ_0 / s	(3.56 ± 2.71) × 10^{-8}	3.56 × 10^{-8}	3.56 × 10^{-8}
U_{eff} / K	11.7 ± 0.6	11.7	11.7
C' / s K^{-n}	0.325 ± 1.47	-	-
B_1 / B^{-2}	0.225 ± 0.181	-	-
B_2 / B^{-2}	(2.26 ± 0.60) × 10^3	-	-
C / s K^{-n}	-	0.325	9.68
n	7 (fixed)	7 (fixed)	7 (fixed)
D_1 / s^{-1}	(5.00 ± 0.20) × 10^3	-	-
D_2 / T^2	(2.39 ± 1.22) × 10^4	-	-
τ_{QTM} / s	-	3.47 × 10^{-2}	6.90 × 10^5

References

1 J. H. Van Vleck, *Phys. Rev.*, 1940, **57**, 426–447.

2 R. Orbach, *Proc. Phys. Soc.*, 1961, **77**, 821–826.

3 A. Fort, A. Rettori, J. Villain, D. Gatteschi and R. Sessoli, *Phys. Rev. Lett.*, 1998, **80**, 612–615.